IEEE Access
Multidisciplinary | Rapid Review | Open Access Journal

Received February 18, 2021, accepted March 9, 2021, date of publication March 12, 2021, date of current version March 22, 2021.

Digital Object Identifier 10.1109/ACCESS.2021.3065692

Bidirectional Power Flow Control Integrated With Pulse and Sinusoidal-Ripple-Current Charging Strategies for Three-Phase Grid-Tied Converters

CHENG-YU TANG[1], (Member, IEEE), PON-TZU CHEN[2], AND JIA-HE JHENG[1]
[1]Department of Electrical Engineering, National Taipei University of Technology, Taipei 10608, Taiwan
[2]Department of Electrical Engineering, National Taiwan University, Taipei 10617, Taiwan

Corresponding author: Cheng-Yu Tang (cytang@ntut.edu.tw)

ABSTRACT The objective of this paper is to propose bidirectional charging/discharging strategies for three-phase grid-tied converters. The bidirectional power flow control feature of the converter is able to realize both charging and discharging capability. Besides, in order to achieve high charging efficiency as well as extend the life of the battery, five charging strategies are adopted and developed: 1) the constant current (CC) charging, 2) the pulse-ripple-current (PRC) charging, 3) the sinusoidal-ripple-current (SRC) charging, 4) the bidirectional pulse-ripple-current (BPRC) charging and 5) the bidirectional sinusoidal-ripple-current (BSRC) charging. The direct quadrature (d-q) transformation is utilized for the converter to realize different charging methods. These methods can be achieved by the digital signal processor (DSP) without adding extra circuit components. In addition, the charging power differences between each strategy are considered and analyzed in this paper. Finally, both simulation and experimental results obtained from a 5-kW prototype circuit verify the performance and feasibility of the proposed bidirectional charger.

INDEX TERMS Three-phase grid-tied converter, bidirectional chargers, energy storage system.

I. INTRODUCTION

Over the past few decades, novel energy technologies such as renewable energy generation systems, electric vehicles and advanced consumer electronics have been rapidly developed to deal with the fossil fuel usage and carbon dioxide emission issues [1]–[4]. Besides, the battery module usually exists in these applications for energy storage [5]–[7]. In order to transfer the electric energy between the battery and the grid, a grid-tied DC-AC converter is necessary while the three-phase H-bridge circuit is one of the most commonly used topologies for high power applications [8]–[12]. In addition, the bidirectional power flow control of the converter is also an essential function to realize both charging and discharging ability for the battery [13]–[15]. The droop-based charging/discharging is also an important mode whereas it was discussed in [16]. Moreover, the bidirectional charger has become an essential component for the electric vehicle (EV) applications [17]–[20].

In order to increase the charging performance as well as extend the battery life, various kinds of charging techniques have been presented [21], [22]. Typically, the constant-current constant-voltage (CC-CV) charging is one of the most commonly adopted charging methods. As soon as the battery voltage is lower than its predefined value, the CC charging will be selected. On the contrary, the CV charging will be chosen as soon as the battery voltage is higher than the predefined value. Although the CC-CV charging can realize the fast charging, the over-heat phenomenon caused by the continuous charging current might damage electrode plates as well as shorten the life of the battery. In view of this, the pulse-ripple-current charging (PRC) and the sinusoidal-ripple-current charging (SRC) technologies were developed [23]. Because of the zero charging current period feature of the PRC and SRC, electron ions in the battery is able to be homogeneous distributed. In other words, the charging stability and the battery life can be increased. Moreover, a modified PRC charging, the Reflex^{TM} concept, was developed [24]. In comparison with the conventional PRC charging, the negative charging period will be included in the Reflex^{TM} method. According to [25], the negative charging period is able to not only stable the chemical reaction of the battery but enhance the uniform distribution of electrolyte concentration. Besides, the Reflex^{TM} charging was utilized for the sealed

The associate editor coordinating the review of this manuscript and approving it for publication was Yonghao Gui.

lead-acid batteries of electric vehicle [26]. The similar bidirectional charging concept can also be adopted for the SRC charging [27].

Some literatures focused on the control and analysis of the PRC and SRC charging techniques [28]–[32]. First, the SRC charging strategy and optimal charging frequency study for Li-ion batteries were proposed in [28]. The battery impedance analysis considering DC component in SRC charging was presented in [29]. Referring to [30], a two-stage Z-source resonant wireless charger with line frequency sinusoidal charging was proposed. Besides, [31] presented an online tracking algorithm to allocate and track the optimal charging frequency for common batteries in real time under any condition. In addition, challenges of the SRC charging of Li-ion batteries were proposed in [32]. Although these proposed methods are effective, the bidirectional power flow control combining the PRC and SRC methods integrated with the three-phase converter are not considered and exposed. In [33], a three-Phase battery charger with the CC and the PRC charging was proposed. However, the SRC charging feature was not considered whereas the bidirectional charging/discharging capability was not developed.

Therefore, the aim of this paper is to propose bidirectional charging/discharging strategies for three-phase grid-tied converters. Main innovations can be summarized as: 1) develop a three-phase AC-DC converter with bidirectional power flow control, 2) integrate charging/discharging strategies with the proposed charger, 3) reveal detailed control concepts and operational principles with mathematical derivations and 4) propose the charging power analysis of different charging strategies. It is worth mentioning that these methods can be realized by the digital signal processor (DSP) without adding extra circuit components. Finally, a 5kW prototype circuit with both simulation and experimental results demonstrate the performance and feasibility of the proposed charging strategies.

II. CIRCUIT CONFIGURATIONS AND BASIC CHARGING CONCEPTS

The circuit diagram and control blocks of the proposed three-phase grid-tied converter are shown in Fig. 1. The dc side of the converter is connected to the battery module while the ac side is connected to the grid. In order to simplify the control of the three-phase converter as well as to achieve different charging strategies, the direct-quadrature (d-q) transformation is a commonly adopted method to control the three-phase converter [34]. Besides, a voltage modulated direct power control was proposed in [35], [36]. It does not need phase-locking and exhibits similar control performance with voltage oriented (d-q) control methods. Therefore, in this paper, the d-q control concept is utilized to achieve the bidirectional power charging strategies. First, the three-phase voltages and currents should be transferred as directed axis voltage and current components, V_d and I_d, and the quadrature axis voltage and current, V_q and I_q via the d-q transformation block. Therefore, the complex power of the three-phase converter,

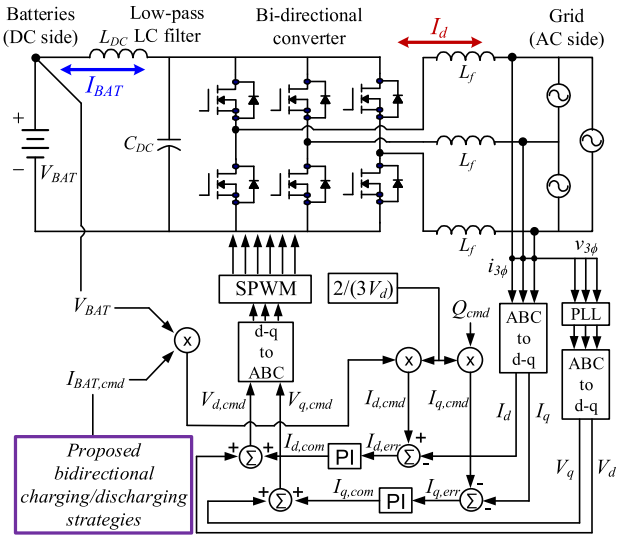

FIGURE 1. The circuit diagram and control blocks.

S, can be expressed as:

$$S = {}^{3}/_{2}\left[\left(V_d I_d + V_q I_q\right) + j\left(V_q I_d - V_d I_q\right)\right]. \tag{1}$$

If the phase-locked-loop (PLL) is utilized to fix the voltage signals on the d-axis, V_q will be zero. Thus, the active power, P, and reactive power, Q, can be obtained as:

$$P_{ac} = {}^{3}/_{2} V_d I_d \tag{2}$$

$$Q_{ac} = -{}^{3}/_{2} V_d I_q. \tag{3}$$

By the arrangement of Eq. (2) and (3), the output active and reactive current command, $I_{d,cmd}$ and $I_{q,cmd}$, can be written as:

$$I_{d,cmd} = {}^{2}/_{3V_d} \times P_{ac} \tag{4}$$

$$I_{q,cmd} = -{}^{2}/_{3V_d} \times Q_{ac}. \tag{5}$$

In order to control the energy between the battery module and the grid, the charging/discharging current of the battery, I_{BAT}, should be well regulated, which can be expressed as a function of the dc-side power, P_{dc}, and the battery voltage, V_{BAT}, as Eq. (6) shows.

$$I_{BAT} = I_{dc} = \frac{P_{dc}}{V_{BAT}}. \tag{6}$$

According to the law of conservation of energy, the dc-side power, P_{dc}, should be equal to the ac side power, P_{ac}, which can be written as:

$$P_{dc} = P_{ac}. \tag{7}$$

It is worth mentioning that in order to simply the analyzations, power losses of the converter are not considered in Eq. (7).

By rearranging Eq. (4), (6) and (7), I_{BAT} can be driven as:

$$I_{BAT} = \frac{P_{ac}}{V_{BAT}} = \frac{3}{2}\frac{V_d \times I_{d,cmd}}{V_{BAT}}. \tag{8}$$

One of the main aims of this paper is to regulate I_{BAT} via $I_{d,cmd}$. Therefore, it can be confirmed that I_{BAT} and $I_{d,cmd}$ can be expressed as a function of K, as:

$$I_{BAT} = K \times I_{d,cmd}, \text{ where } K = \frac{3V_d}{2V_{BAT}}. \tag{9}$$

As a result, the charging and discharging current of the battery can be controlled by the d-axis current command of the three-phase converter.

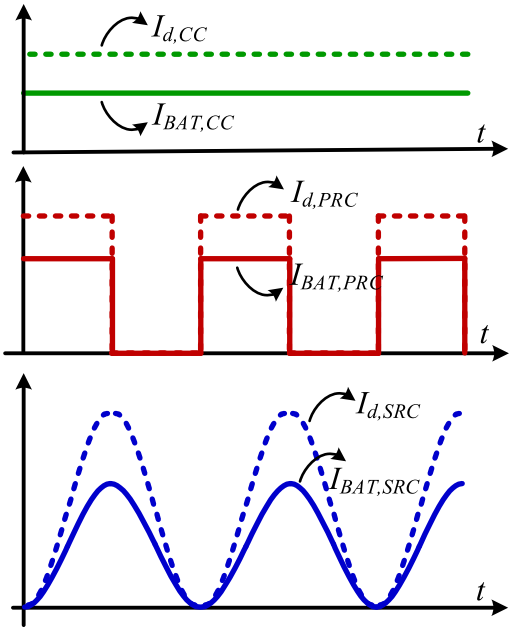

FIGURE 2. Conceptual diagrams of the relations between I_d and I_{BAT} of (a) The CC charging (b) The PRC charging (c) The SRC charging.

Conceptual diagrams of the relations between I_d and I_{BAT} of the CC, the PRC and the SRC charging are shown in Fig. 2. According to the previous derivations, the battery current, $I_{BAT,CC}$, and the d-axis current, $I_{d,CC}$, under the CC charging mode can be written as:

$$I_{BAT,CC} = K \times I_{d,CC}. \tag{10}$$

On the other hand, the battery current, $I_{BAT,PRC}$, and the d-axis current, $I_{d,PRC}$, under the PRC charging can be expressed as:

$$\begin{aligned} I_{BAT,PRC} &= K \times I_{d,PRC}, \\ \text{where } I_{d,PRC} &= \begin{cases} I_{PRC,peak}, t_o \le t < t_1 \\ 0, t_1 \le t < t_2. \end{cases} \end{aligned} \tag{11}$$

Finally, the battery current, $I_{BAT,SRC}$, and the d-axis current, $I_{d,SRC}$, under the SRC charging can be derived as:

$$\begin{aligned} I_{BAT,SRC} &= K \times I_{d,SRC}, \\ \text{where } I_{d,SRC} &= \frac{1}{2}\left[I_{SRC,peak}\sin(\omega t) + I_{SRC,peak}\right]. \end{aligned} \tag{12}$$

III. PROPOSED BIDIRECTIONAL CHARGING/DISCHARGING STRATEGIES

In order to further enhance the charging performance as well as extend the life of the battery, the bidirectional charging/discharging strategies are proposed. Both of the PRC and SRC cases are considered and realized via the three-phase grid-tied converter. In addition, analysis of the charging power differences between each charging method will also be presented in this section.

A. THE PROPOSED BPRC AND BSRC CHARGING

Fig. 3 shows the bidirectional charging/discharging concept for the PRC and SRC. First, the Reflex charging method [37] is adopted for the bidirectional PRC (BPRC) charging, as shown in Fig. 3(a). It can be confirmed that there are three charging states: 1) the charging period, 2) the zero current period and 3) the discharging period. During the charging period, the converter is operated in AC-DC power factor correction (PFC) mode. In this mode, the energy will be transferred form the grid to the battery. On the contrary, during the discharging period, the converter is operated in DC-AC inverter mode as well as transfer the battery energy to the grid.

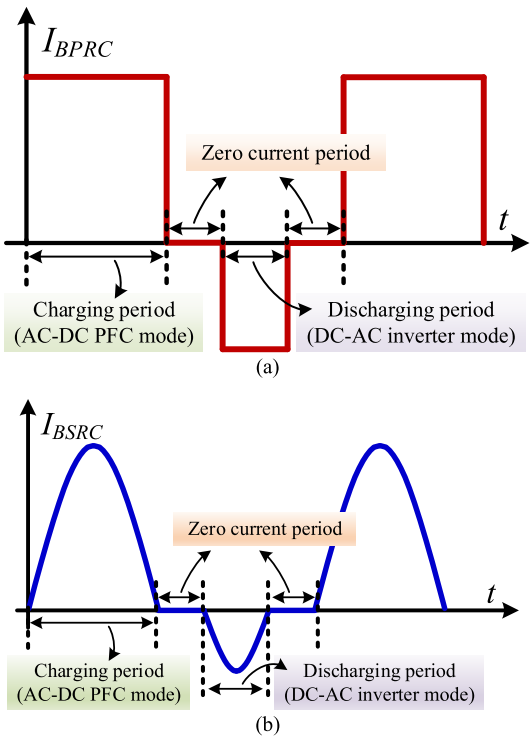

FIGURE 3. The proposed bidirectional charging/discharging strategies (a) The BPRC charging (b) The BSRC charging.

On the other hand, the conceptual diagram of the bidirectional SRC (BSRC) charging is shown in Fig. 3(b). Similar with the BPRC, there are also three charging states, including the charging, zero current and discharging period of the BSRC. It is worth mentioning that the control of both BPRC

and BSRC can be realized by the DSP. Besides, the maximum charging/discharging current and the charging/discharging period can be determined by the engineers.

B. THE CHARGING POWER ANALYSIS

The proposed PRC, SRC, BPRC and BSRC charging strategies controlled via the bidirectional three-phase converter is able to homogeneous distribute the electron ions as well as extend the life of the battery. However, the charging power might be decreased because of nonlinear charging current characteristics. Therefore, the charging power difference between each charging strategy should be considered and analyzed.

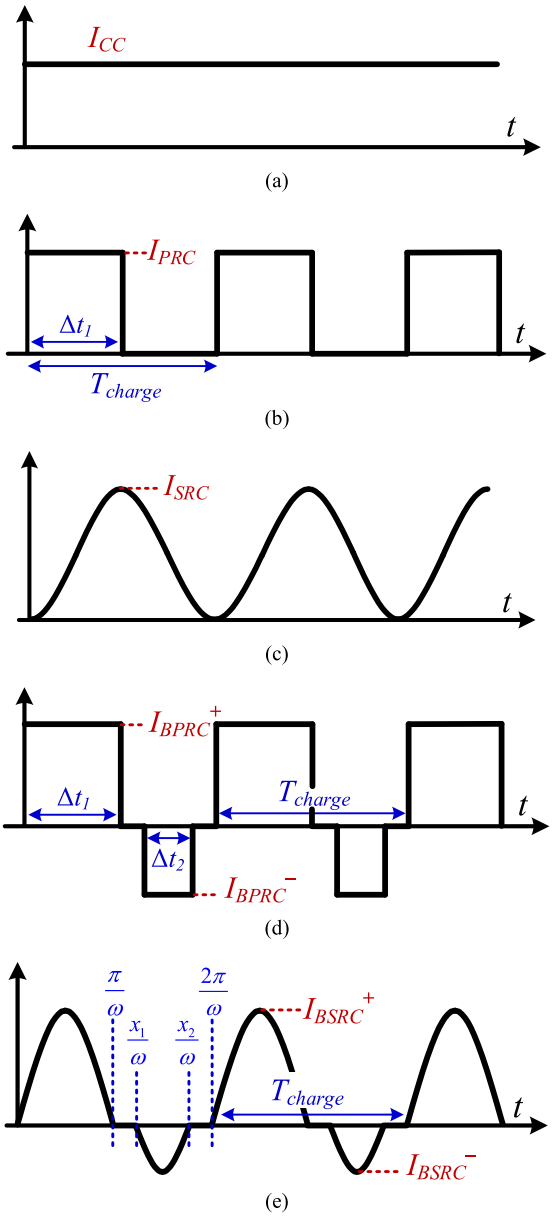

FIGURE 4. Conceptual diagrams of the charging current with different strategies (a) The CC charging (b) The PRC charging (c) The SRC charging (d) The BPRC charging (e) The BSRC charging.

Fig. 4 shows the conceptual diagram of the charging current with different strategies. First, Fig. 4(a) shows the current waveform with the CC charging while the PRC charging waveform is shown in Fig. 4(b). The charging power of the PRC charging, P_{PRC}, can be expressed as:

$$P_{PRC} = V_{BAT} \times I_{PRC,avg} = V_{BAT} \times \left(\frac{I_{PRC} \times \Delta t}{T_{charge}} \right), \quad (13)$$

while $I_{PRC,avg}$ is the average current of the PRC charging. I_{PRC} represents the peak charging current. Δt is the positive charging period whereas T_{charge} represents the total charging period.

Therefore, the charging power difference between the CC and the PRC charging, ΔP_{CC-PRC}, can be written as:

$$\begin{aligned} \Delta P_{CC-PRC} &= P_{CC} - P_{PRC} \\ &= V_{BAT} \left[I_{CC} - \left(\frac{I_{PRC} \times \Delta t}{T_{charge}} \right) \right], \end{aligned} \quad (14)$$

while P_{CC} and I_{CC} represent the power and current with the CC charging, respectively. If I_{PRC} is equal to I_{CC}, ΔP_{CC-PRC} can be modified as:

$$\Delta P_{CC-PRC} = V_{BAT} \times I_{CC} \times \left(\frac{T_{charge} - \Delta t}{T_{charge}} \right). \quad (15)$$

According to Fig. 4(c), the charging power with the SRC charging method, P_{SRC}, can be defined as:

$$P_{SRC} = V_{BAT} \times I_{SRC,avg} = V_{BAT} \times \frac{1}{2} I_{SRC}, \quad (16)$$

while I_{SRC} is the maximum SRC charging current. $I_{SRC,avg}$ represents the average SRC charging current, which is equal to 50% of I_{SRC}.

Besides, the charging power difference between the CC and the SRC charging, ΔP_{CC-SRC}, can be written as:

$$\Delta P_{CC-SRC} = P_{CC} - P_{SRC} = V_{BAT} \left[I_{CC} - \frac{1}{2} I_{SRC} \right]. \quad (17)$$

If I_{SRC} is set as I_{CC}, ΔP_{CC-SRC} can be calculated as:

$$\Delta P_{CC-SRC} = \frac{1}{2} \times V_{BAT} \times I_{CC} = \frac{1}{2} P_{CC}. \quad (18)$$

Fig. 4(d) shows the scenario of the BPRC charging strategy whereas the BPRC charging power, P_{BPRC}, can be expressed as:

$$\begin{aligned} P_{BPRC} &= V_{BAT} \times I_{BPRC,avg} = V_{BAT} \\ &\times \left(\frac{I_{BPRC}^{+} \Delta t_1 - I_{BPRC}^{-} \Delta t_2}{T_{charge}} \right), \end{aligned} \quad (19)$$

while $I_{BPRC,avg}$ is the average BPRC charging current. I_{BPRC}^{+} and I_{BPRC}^{-} are the peak positive charging current and peak negative charging current, respectively. Δt_1 and Δt_2 represent the positive charging period and negative charging period, respectively.

The charging power difference between the CC and the BPRC charging, $\Delta P_{CC-BPRC}$, can be calculated as:

$$\Delta P_{CC-BPRC} = P_{CC} - P_{BPRC}$$

$$= V_{BAT}\left[I_{CC} - \left(\frac{I^{+}_{BPRC}\Delta t_1 - I^{-}_{BPRC}\Delta t_2}{T_{charge}}\right)\right]. \tag{20}$$

If I^{+}_{BPRC} and I^{-}_{BPRC} are equal to I_{CC}, $\Delta P_{CC-BPRC}$ can be determined as:

$$\Delta P_{CC-BPRC} = V_{BAT} \times I_{CC} \times \left(\frac{T_{charge} - \Delta t_1 + \Delta t_2}{T_{charge}}\right). \tag{21}$$

Finally, the BSRC charging scenario is shown in Fig. 4(e). The BSRC charging power, P_{BSRC}, can be written as:

$$P_{BSRC} = V_{BAT} \times I_{BSRC,avg}. \tag{22}$$

while $I_{BSRC,avg}$ is the average BSRC charging current, which can be defined as:

$$I_{BSRC,avg} = \frac{\int_0^{\pi/\omega} I^{+}_{BSRC}\sin\omega t dt - \int_{x_1/\omega}^{x_2/\omega} I^{-}_{BSRC}\sin\omega t dt}{T_{charge}/2}. \tag{23}$$

In Eq. (23), I^{+}_{BSRC} and I^{-}_{BSRC} are the maximum positive and negative charging current, respectively. ω is the angular frequency of the charging current, which is equal to $2\pi f$. x_1 and x_2 represent the starting and stopping angle of the discharging period. It should be noticed that x_1 should be within the range of π and $3\pi/2$. x_2 should be within the range of $3\pi/2$ and 2π, as:

$$\pi \le x_1 \le 3\pi/2;\ 3\pi/2 \le x_2 \le 2\pi. \tag{24}$$

Eventually, the charging power difference between the CC and the BSRC charging, $\Delta P_{CC-BSRC}$, can be calculated as:

$$\Delta P_{CC-BSRC} = P_{CC} - P_{BSRC} = V_{BAT}\left[I_{CC} - I_{BSRC,avg}\right]. \tag{25}$$

The definition of ΔP_{CC-PRC}, ΔP_{CC-SRC}, $\Delta P_{CC-BPRC}$ and $\Delta P_{CC-BSRC}$ are given in this section. From the analysis, it can be confirmed that the average charging power of the PRC, SRC, BPRC, BSRC charging will be lower than the CC charging. In other words, compare to the CC charging, the charging period with the four different charging strategies will be longer. Moreover, because of the zero and negative charging period, the required charging time of the BPRC and BSRC charging will be greater than the required charging time of the PRC and SRC charging, respectively. Therefore, longer charging time will be the main disadvantages of the PRC, SRC, BPRC, BSRC charging methods.

However, according to [25], the negative charging period is able to stable the chemical reaction of the battery as well as to enhance the uniform distribution of electrolyte concentration. In other words, main advantages of the PRC, SRC, BPRC, BSRC charging are to decrease the battery rising temperature and to increase the battery life.

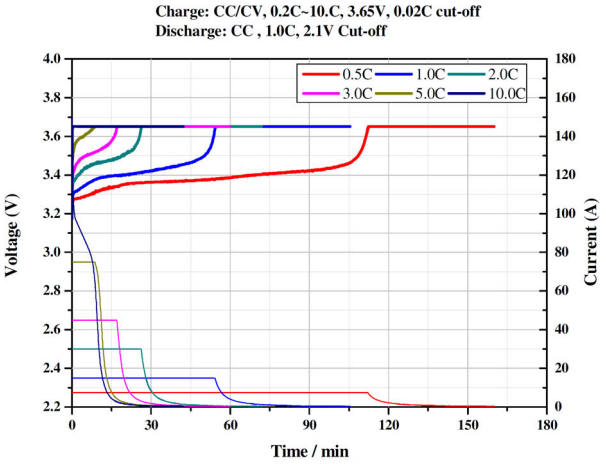

(a)

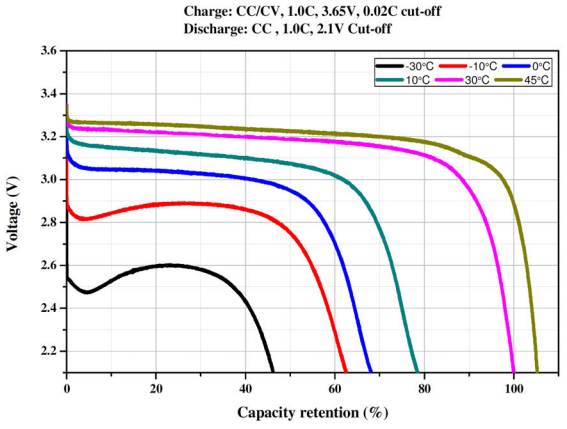

(b)

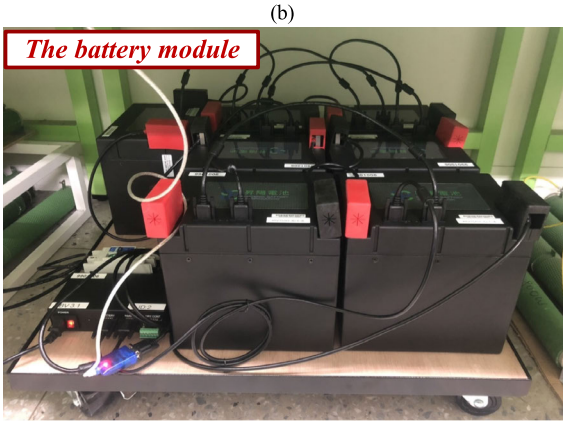

(c)

FIGURE 5. Characteristic curves and figures of the LiFePO4 battery. (a) The charging characteristic curves of the battery cell (b) The temperature characteristic curves of the battery cell (c) The figure of the battery module.

IV. SIMULATION AND EXPERIMENTAL VALIDATIONS

To verify the performance and feasibility of the proposed strategies, a 5kW prototype circuit of the three-phase grid-tied converter is designed and implemented. Specifications of the circuit are shown in Table 1. The dc-side voltage and current are set as 400V and 12.5A, respectively. The ac-side of the converter is connected to the 3-phase, $220V_{rms}$, 60Hz system with the three-phase output currents are $13A_{rms}$.

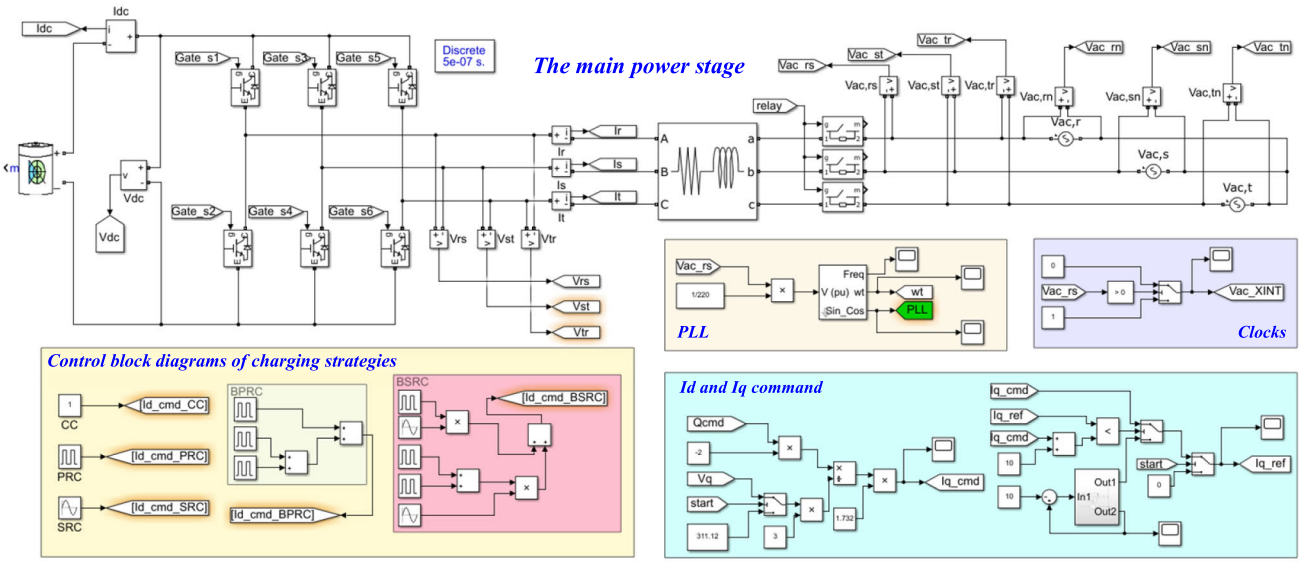

FIGURE 6. The main circuit and control block diagrams in Matlab/simulink.

TABLE 1. Specifications of the prototype three-phase grid-tied inverter.

Parameters	Value
Rated power	5-kW
Input normal battery voltage ($V_{bat,nor}$)	400V
Rated input current (I_{in})	12.5A
Grid voltages (Line-to-Line)	3-phase, 220V_{rms}, 60Hz
Rated output current	3-phase, 13A $_{rms}$, 60Hz
Switches	H1M065F020 (SiC MOSFET)
Switching frequency	50kHz
Gate driver IC for the switches	TLP350
Input inductance, L_{in}	100μH
Input capacitance, C_{in}	1.36mF
Output inductance, L_f	2mH
System controller	DSP TMS320F28335

On the other hand, the SiC MOSFETs have been widely adopted for power electronics due to the characteristics of the high breakdown voltage, low drain-to-source resistance and high heat dissipation rate [38], [39]. Besides, there will be no current-tail effect on the SiC MOSFET. Therefore, the switching frequency and the circuit efficiency can be increased while the switching losses can be decreased. Eventually, the SiC MOSFET is suitable for high power and high frequency applications. Therefore, the Silicon-carbide MOSFET, H1M065F020 is chosen as main switches whereas the switching frequency is determined as 50kHz.

It is worth mentioning that the DSP TMS320F28335 made by Texas Instruments is utilized as the system controller to realize the proposed charging strategies. The dc-side inductance and capacitance, L_{in}, and C_{in}, are calculated as 100μH and 1.36mF, respectively, to filter out the high frequency current component on the dc-side. Besides, the ac-side inductance, L_f, is set as 2mH. In order to verify the proposed bidirectional battery charger, the LiFePO4 battery module made by *Phoenix Silicon International Corporation* is adopted. Fig. 5(a) and Fig. 5(b) show the charging characteristic curves, the temperature characteristic curves, respectively [40]. The figure of the battery module is shown in Fig. 5 (c).

In the following, both simulation and experimental results are presented.

A. SIMULATION RESULTS

The proposed charging strategies are first verified via the Matlab/Simulink. Fig. 6 shows the main circuit and control block diagrams with the proposed bidirectional charging strategies. Simulation results of V_{BAT}, I_{BAT}, $I_{d,cmd}$, the three-phase ac currents, I_{ac}, and the three-phase ac voltages, V_{ac}, with different charging methods are shown in Fig. 7.

First, Fig. 7(a) shows waveforms of the CC charging. Due to the CC charging feature, V_{BAT}, I_{BAT} and $I_{d,cmd}$ remain constant values. Waveforms of the PRC charging are shown in Fig. 7(b). In this scenario, I_{BAT} and $I_{d,cmd}$ are controlled with pulse form. In the meantime, I_{ac} currents are changed between zero and its peak value. Then, Fig. 7(c) shows results of the SRC charging. It can be seem that I_{BAT} and $I_{d,cmd}$ are regulated with sinusoidal form while I_{ac} currents are also fluctuated with the SRC charging frequency. It can be confirmed that the I_{ac} currents consist of two different frequency, which are: (1) the SRC charging frequency and (2) the ac line frequency. It should be noticed that the SRC charging frequency must be lower than the ac line frequency to prevent the dc-side charging current distortion.

Finally, simulation waveforms of the BPRC and BSRC charging are shown in Fig. 7(d) and Fig. 7(e), respectively.

Different from the results of PRC and SRC charging, there will be both charging and discharging period for the BPRC

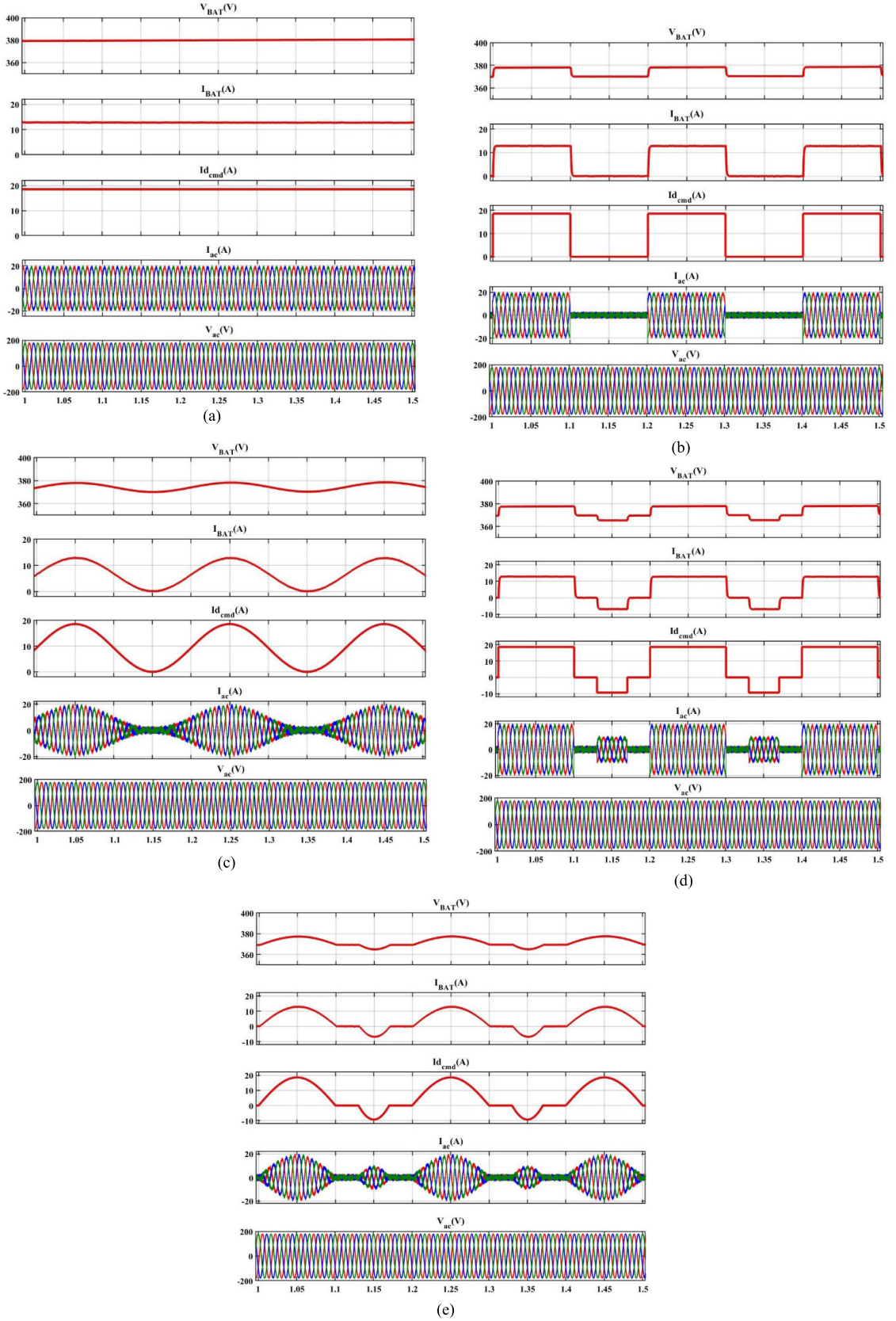

FIGURE 7. Simulation waveforms of the V_{BAT}, I_{BAT}, $I_{d,cmd}$, I_{ac} and V_{ac} with different charging strategies (a) The CC charging (b) The PRC charging (c) The SRC charging (d) The BPRC charging (e) The BSRC charging.

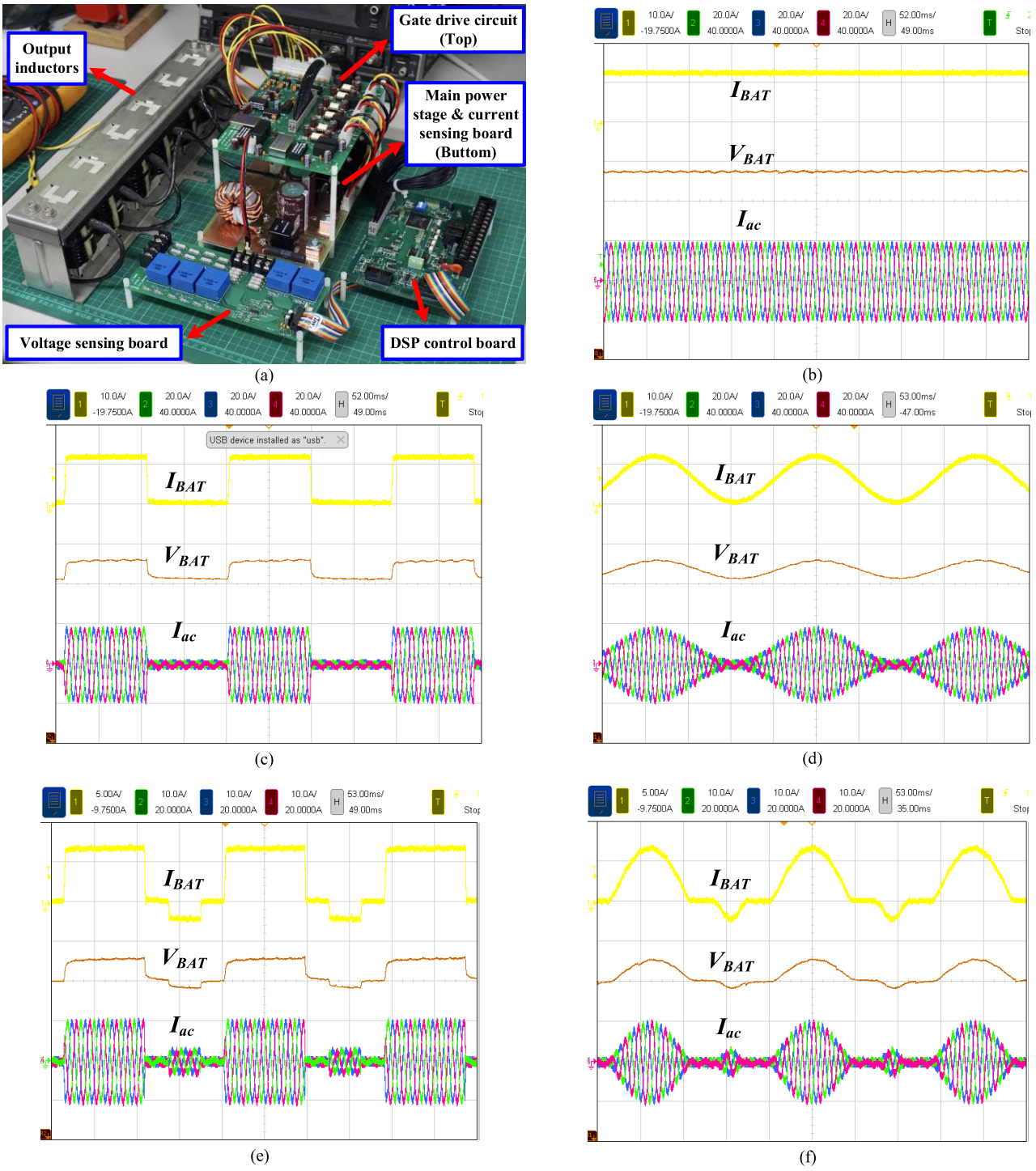

FIGURE 8. Experimental results of the proposed circuit and charging strategies (a) The prototype circuit figure (b) The CC charging (c) The PRC charging (d) The SRC charging (e) The BPRC charging (f) The BSRC charging.

and BSRC charging. In other words, the bidirectional power flow control should be considered and realized by the converter in these two scenarios. During the charging period, the converter is operated in AC-DC (PFC) mode to extract power from the grid to the battery. On the contrary, the converter will be operated in DC-AC (inverter) mode during the discharging period.

B. EXPERIMENTAL VERIFICATIONS

Fig. 8 shows the experimental results of the proposed circuit and charging strategies. First, the prototype circuit figure of the three-phase grid-tied converter is shown in Fig. 8(a). The circuit can be divided into five parts, including the main power stage and current sensing board, the gate drive board, the voltage sensing board, the DSP control

board and output inductors. It is worth mentioning that the Silicon-Carbide (SiC) MOSFETs are adopted in the main power stage. Besides, on the DSP-based control circuit, the TMS320F28335 chip is utilized as the system controller.

Fig. 8(b) shows experimental waveforms of V_{BAT}, I_{BAT}, and I_{ac} under the CC charging. In this test, I_{ac} are controlled as $13A_{rms}$ whereas I_{BAT} can be calculated as 12.5A according to Eq. (10). It should be noticed that the converter is operated in 5kW full-load condition. Experimental waveforms of V_{BAT}, I_{BAT}, and I_{ac} under the PRC charging are shown in Fig. 8(c). Because of the pulse charging feature, I_{BAT} are controlled with pulse form while I_{ac} are changed between zero and its peak value. Besides, Fig. 8(d) shows experimental results of the SRC charging. It can be seem that I_{BAT} and V_{BAT} are regulated with sinusoidal form. I_{ac} currents are fluctuated with the SRC charging frequency.

Finally, experimental results of the BPRC and BSRC are shown in Fig. 8(e) and Fig. 8(f), respectively. These two scenarios demonstrate the bidirectional power flow control capability. During the charging period, the converter is operated in AC-DC (PFC) mode and the power flows from the grid to the battery. On the contrary, the converter is operated in DC-AC (inverter) mode during the discharging period and the power flows form the battery to the grid.

It can be confirmed that experiments demonstrate the same results of simulations. Therefore, the performance and feasibility of the proposed circuit and charging strategies can be verified.

V. CONCLUSION

This paper proposes a bidirectional three-phase grid-tied converter with charging/discharging strategies. The converter is able to be operated in the AC-DC (PFC) mode and the DC-AC (inverter) mode to realize the bidirectional power flow control feature. In order to increase the charging efficiency as well as extend the battery life, five charging strategies are considered and developed. Main contributions of this paper can be concluded as: 1) a three-phase AC-DC converter with bidirectional power flow control is developed, 2) five charging/discharging strategies are integrated with the proposed charger, 3) detailed control concepts and operational principles are revealed with mathematical derivations and 4) the charging power analysis of different charging strategies is presented.

These charging methods can be achieved by the proposed bidirectional converter with the d-q transformation concept. Moreover, comprehensive analysis and mathematical derivations of the charging power differences between each strategy are presented. Finally, both simulation and experimental results obtained from a 5-kW prototype demonstrate the performance and feasibility of the proposed bidirectional charger.

ACKNOWLEDGMENT

The authors would like to thank the invaluable support with the experimental setup from the Electric Energy Processing Laboratory (EEPro), Department of Electrical Engineering, National Taiwan University.

REFERENCES

[1] K. Thirugnanam, S. K. Kerk, C. Yuen, N. Liu, and M. Zhang, "Energy management for renewable microgrid in reducing diesel generators usage with multiple types of battery," *IEEE Trans. Ind. Electron.*, vol. 65, no. 8, pp. 6772–6786, Aug. 2018.

[2] P. B. L. Neto, O. R. Saavedra, and L. A. de Souza Ribeiro, "A dual-battery storage bank configuration for isolated microgrids based on renewable sources," *IEEE Trans. Sustain. Energy*, vol. 9, no. 4, pp. 1618–1626, Oct. 2018.

[3] U. Manandhar, N. R. Tummuru, S. K. Kollimalla, A. Ukil, G. H. Beng, and K. Chaudhari, "Validation of faster joint control strategy for battery- and supercapacitor-based energy storage system," *IEEE Trans. Ind. Electron.*, vol. 65, no. 4, pp. 3286–3295, Apr. 2018.

[4] F. Wu, X. Li, F. Feng, and H. B. Gooi, "Multi-topology-mode grid-connected inverter to improve comprehensive performance of renewable energy source generation system," *IEEE Trans. Power Electron.*, vol. 32, no. 5, pp. 3623–3633, May 2017.

[5] Z. Zhang, Y.-Y. Cai, Y. Zhang, D.-J. Gu, and Y.-F. Liu, "A distributed architecture based on microbank modules with self-reconfiguration control to improve the energy efficiency in the battery energy storage system," *IEEE Trans. Power Electron.*, vol. 31, no. 1, pp. 304–317, Jan. 2016.

[6] S. Dey, Y. Shi, K. Smith, A. Colclasure, and X. Li, "From battery cell to electrodes: Real-time estimation of charge and health of individual battery electrodes," *IEEE Trans. Ind. Electron.*, vol. 67, no. 3, pp. 2167–2175, Mar. 2020.

[7] D. Varajão, R. E. Araújo, L. M. Miranda, and J. A. P. Lopes, "Modulation strategy for a single-stage bidirectional and isolated AC–DC matrix converter for energy storage systems," *IEEE Trans. Ind. Electron.*, vol. 65, no. 4, pp. 3458–3468, Apr. 2018.

[8] C.-Y. Tang, Y.-F. Chen, Y.-M. Chen, and Y.-R. Chang, "DC-link voltage control strategy for three-phase back-to-back active power conditioners," *IEEE Trans. Ind. Electron.*, vol. 62, no. 10, pp. 6306–6316, Oct. 2015.

[9] J. P. R. A. Méllo and C. B. Jacobina, "Asymmetrical cascaded three-phase AC–DC converters with injection transformers," *IEEE Trans. Ind. Appl.*, vol. 55, no. 3, pp. 2800–2812, Jun. 2019.

[10] M. M. Hasan, A. Abu-Siada, and M. S. A. Dahidah, "A three-phase symmetrical DC-link multilevel inverter with reduced number of DC sources," *IEEE Trans. Power Electron.*, vol. 33, no. 10, pp. 8331–8340, Oct. 2018.

[11] G. Farivar, B. Hredzak, and V. G. Agelidis, "A DC-side sensorless cascaded H-bridge multilevel converter-based photovoltaic system," *IEEE Trans. Ind. Electron.*, vol. 63, no. 7, pp. 4233–4241, Jul. 2016.

[12] H. Salimian and H. Iman-Eini, "Fault-tolerant operation of three-phase cascaded H-bridge converters using an auxiliary module," *IEEE Trans. Ind. Electron.*, vol. 64, no. 2, pp. 1018–1027, Feb. 2017.

[13] B. Mangu, S. Akshatha, D. Suryanarayana, and B. G. Fernandes, "Grid-connected PV-wind-battery-based multi-input transformer-coupled bidirectional DC–DC converter for household applications," *IEEE J. Emerg. Sel. Topics Power Electron.*, vol. 4, no. 3, pp. 1086–1095, Sep. 2016.

[14] R. Baranwal, K. V. Iyer, K. Basu, G. F. Castelino, and N. Mohan, "A reduced switch count single-stage three-phase bidirectional rectifier with high-frequency isolation," *IEEE Trans. Power Electron.*, vol. 33, no. 11, pp. 9520–9541, Nov. 2018.

[15] D. Sha, G. Xu, and Y. Xu, "Utility direct interfaced charger/discharger employing unified voltage balance control for cascaded H-bridge units and decentralized control for CF-DAB modules," *IEEE Trans. Ind. Electron.*, vol. 64, no. 10, pp. 7831–7841, Oct. 2017.

[16] R. Wang, Q. Sun, W. Hu, Y. Li, D. Ma, and P. Wang, "SoC-based droop coefficients stability region analysis of the battery for stand-alone supply systems with constant power loads," *IEEE Trans. Power Electron.*, vol. 36, no. 7, pp. 7866–7879, Jul. 2021.

[17] N. Tashakor, E. Farjah, and T. Ghanbari, "A bidirectional battery charger with modular integrated charge equalization circuit," *IEEE Trans. Power Electron.*, vol. 32, no. 3, pp. 2133–2145, Mar. 2017.

[18] X. Wang, C. Jiang, B. Lei, H. Teng, H. K. Bai, and J. L. Kirtley, "Power-loss analysis and efficiency maximization of a silicon-carbide MOSFET-based three-phase 10-kW bidirectional EV charger using variable-DC-bus control," *IEEE J. Emerg. Sel. Topics Power Electron.*, vol. 4, no. 3, pp. 880–892, Sep. 2016.

[19] H. Li, Z. Zhang, S. Wang, J. Tang, X. Ren, and Q. Chen, "A 300-kHz 6.6-kW SiC bidirectional LLC onboard charger," *IEEE Trans. Ind. Electron.*, vol. 67, no. 2, pp. 1435–1445, Feb. 2020.
[20] H. N. de Melo, J. P. F. Trovão, P. G. Pereirinha, H. M. Jorge, and C. H. Antunes, "A controllable bidirectional battery charger for electric vehicles with vehicle-to-grid capability," *IEEE Trans. Veh. Technol.*, vol. 67, no. 1, pp. 114–123, Jan. 2018.
[21] K. Noh, M. Zhang, and E. Sánchez-Sinencio, "A unified amplifier-based CC-CV linear charger for energy-constrained low-power applications," *IEEE Trans. Circuits Syst. II, Exp. Briefs*, vol. 66, no. 3, pp. 377–381, Mar. 2019.
[22] L. Patnaik, A. V. J. S. Praneeth, and S. S. Williamson, "A closed-loop constant-temperature constant-voltage charging technique to reduce charge time of lithium-ion batteries," *IEEE Trans. Ind. Electron.*, vol. 66, no. 2, pp. 1059–1067, Feb. 2019.
[23] L.-R. Chen, J.-J. Chen, C.-M. Ho, S.-L. Wu, and D.-T. Shieh, "Improvement of Li-ion battery discharging performance by pulse and sinusoidal current strategies," *IEEE Trans. Ind. Electron.*, vol. 60, no. 12, pp. 5620–5628, Dec. 2013.
[24] C.-M. Lai, Y.-H. Li, Y.-H. Cheng, and J. Teh, "A high-gain reflex-based bidirectional DC charger with efficient energy recycling for low-voltage battery charging-discharging power control," *Energies*, vol. 11, no. 3, p. 623, Mar. 2018.
[25] C.-M. Lai, J. Teh, Y.-H. Cheng, and Y.-H. Li, "A reflex-charging based bidirectional DC charger for light electric vehicle and DC-microgrids," in *Proc. IEEE Region Conf. (TENCON)*, Nov. 2017, pp. 280–284.
[26] T.-W. Wang, M.-J. Yang, K.-K. Shyu, and C.-M. Lai, "Design fuzzy SOC estimation for sealed lead-acid batteries of electric vehicles in reflex TM," in *Proc. IEEE Int. Symp. Ind. Electron.*, Jun. 2007, pp. 95–99.
[27] Y. Zhao, R. Fu, and S. Choe, "Modeling of SEI formation based on a electrochemical reduced erder model for Li(MnNiCo)O2/carbon polymer battery," in *Proc. IEEE VPPC*, Oct. 2015, pp. 1–4.
[28] L.-R. Chen, S.-L. Wu, D.-T. Shieh, and T.-R. Chen, "Sinusoidal-ripple-current charging strategy and optimal charging frequency study for Li-ion batteries," *IEEE Trans. Ind. Electron.*, vol. 60, no. 1, pp. 88–97, Jan. 2013.
[29] S.-Y. Cho, I.-O. Lee, J.-I. Baek, and G.-W. Moon, "Battery impedance analysis considering DC component in sinusoidal ripple-current charging," *IEEE Trans. Ind. Electron.*, vol. 63, no. 3, pp. 1561–1573, Mar. 2016.
[30] H. Zeng, X. Wang, and F. Z. Peng, "High power density Z-source resonant wireless charger with line frequency sinusoidal charging," *IEEE Trans. Power Electron.*, vol. 33, no. 12, pp. 10148–10156, Dec. 2018.
[31] A. A. Hussein, A. A. Fardoun, and S. S. Stephen, "An online frequency tracking algorithm using terminal voltage spectroscopy for battery optimal charging," *IEEE Trans. Sustain. Energy*, vol. 7, no. 1, pp. 32–40, Jan. 2016.
[32] A. Bessman, R. Soares, S. Vadivelu, O. Wallmark, P. Svens, H. Ekstrom, and G. Lindbergh, "Challenging sinusoidal ripple-current charging of lithium-ion batteries," *IEEE Trans. Ind. Electron.*, vol. 65, no. 6, pp. 4750–4757, Jun. 2018.
[33] C.-Y. Tang, P.-T. Chen, and Y.-M. Chen, "A three-phase battery charger with constant current and pulse-ripple-current charging capability," in *Proc. IEEE 4th Int. Future Energy Electron. Conf. (IFEEC)*, Nov. 2019, pp. 1–5.
[34] C.-Y. Tang, C.-J. Tsai, Y.-M. Chen, and Y.-R. Chang, "Dynamic optimal AC line current regulation method for three-phase active power conditioners," *IEEE J. Emerg. Sel. Topics Power Electron.*, vol. 5, no. 2, pp. 901–911, Jun. 2017.
[35] Y. Gui, M. Li, J. Lu, S. Golestan, J. M. Guerrero, and J. C. Vasquez, "A voltage modulated DPC approach for three-phase PWM rectifier," *IEEE Trans. Ind. Electron.*, vol. 65, no. 10, pp. 7612–7619, Oct. 2018.
[36] S. Gao, H. Zhao, Y. Gui, D. Zhou, and F. Blaabjerg, "An improved direct power control for doubly fed induction generator," *IEEE Trans. Power Electron.*, vol. 36, no. 4, pp. 4672–4685, Apr. 2021.
[37] L.-R. Chen, N.-Y. Chu, C.-S. Wang, and R.-H. Liang, "Design of a reflex-based bidirectional converter with the energy recovery function," *IEEE Trans. Ind. Electron.*, vol. 55, no. 8, pp. 3022–3029, Aug. 2008.
[38] H. Li, C. Wang, Y. Liu, and R. Yue, "Research on single-switch wireless power transfer system based on SiC MOSFET," *IEEE Access*, vol. 7, pp. 163796–163805, 2019.
[39] L. Schrittwieser, M. Leibl, M. Haider, F. Thony, J. W. Kolar, and T. B. Soeiro, "99.3% efficient three-phase buck-type all-SiC SWISS rectifier for DC distribution systems," *IEEE Trans. Power Electron.*, vol. 34, no. 1, pp. 126–140, Jan. 2019.
[40] *Rechargeable Lithium-Ion Battery 40138IFA Datesheet*, Phoenix Silicon Int. Corp., Hsinchu, Taiwan, 2014.

CHENG-YU TANG (Member, IEEE) received the B.S. degree in electrical engineering from the National Kaohsiung University of Applied Sciences, Kaohsiung, Taiwan, in 2010, the M.S. degree in electrical engineering from the National Taipei University of Technology, Taipei, Taiwan, in 2012, and the Ph.D. degree from the Department of Electrical Engineering, National Taiwan University, Taipei, in 2016.

He is currently an Associate Professor with the Department of Electrical Engineering, National Taipei University of Technology. His research interests include switching power supplies, renewable energy systems, and power flow control.

PON-TZU CHEN received the B.S. degree in electrical engineering from Feng Chia University, Taichung, Taiwan, in 2017, and the M.S. degree in electrical engineering from National Taiwan University, Taipei, Taiwan, in 2020. She is currently an Application Engineer with Silergy Technology Inc., Kaohsiung, Taiwan. Her current research interests include the power electronics and bidirectional three-phase charger.

JIA-HE JHENG received the B.S. degree in electrical engineering from National Ilan University, Ilan, Taiwan, in 2019. He is currently pursuing the M.S. degree with the Department of Electrical Engineering, National Taipei University of Technology, Taipei, Taiwan. His research interests include applications of switching power supplies, renewable energy systems, and the power flow control.